Available online at www.sciencedirect.com
SCIENCE DIRECT®
Journal of Sound and Vibration 276 (2004) 1043–1063
JOURNAL OF SOUND AND VIBRATION
www.elsevier.com/locate/jsvi

Identification of modal parameters from measured input and output data using a vector backward auto-regressive with exogeneous model

Chen-Far Hung*, Wen-Jiunn Ko, Yen-Tun Peng

Department of Engineering Science and Ocean Engineering, National Taiwan University, No. 1, Sec. 4, Roosevelt Road, Taipei 106, Taiwan

Received 27 March 2003; accepted 15 August 2003

Abstract

This paper proposes a modal identification system based on vector backward auto-regressive with exogeneous (VBARX) model. The model is an extension of vector backward auto-regressive (VBAR). Both the backward models offer the same benefits in selecting physical modes, since both can provide a determinate boundary that separates system modes from spurious modes. The VBAR model can identify the structural parameters from only output data. In some circumstances, if the input data are available, the extended model, VBARX model, provides an additional advantage over the VBAR model. In this study, an equivalent state-space model derived from measured input and output data is transformed from the VBARX model. Consequently, the structural modal parameters can be estimated accurately using the equivalent state-space model. Two examples of modal identification are presented to demonstrate the availability and effectiveness of the proposed VBARX method. (1) Numerical data simulated in a 3-d.o.f. dynamic system with various types of input data and various noise levels. (2) Experimental data obtained from the National Center for Research on Earthquake Engineering (NCREE) in Taiwan, concerning five-story $\frac{1}{2}$-scale steel structure under a shaking table test.

1. Introduction

Various methods for identifying the modal parameters have been developed over the last few decades. Methods of modal identification can be categorized as time-domain method or frequency-domain method. Both types of methods have their merits in extracting modal

*Corresponding author. Department of Naval Architecture and Ocean Engineering, National Taiwan University, 73 Chow-Shan Road, Taipei, Taiwan. Tel.: +886-2-236-25470; fax: +886-2-239-29885.
E-mail address: hungef@ccms.ntu.edu.tw (C.-F. Hung).

0022-460X/$ - see front matter
doi:10.1016/j.jsv.2003.08.020

parameters from measured data. Frequency-domain methods are popular and still predominate engineering practice [1,2]. Time-domain methods are useful for solving problems with many modes and multi-channel measurement, and also for those that involve closely spaced and non-proportional modes. Time-domain methods can directly be applied to the measured response data; hence, this paper focused on time-domain methods.

Works on time-domain methods appeared in the late 1970s; these early versions included the Ibrahim time domain method [3,4] and the polyreference method [5–7]. The eigensystem realization algorithm (ERA) of Juang and Pappa [8,9] can determine a state-space model from impulse responses. Van Overschee and De Moore proposed the numerical algorithms for subspace state-space system identification (N4SID) [10], and Verhaegen and Dewilde proposed the multivariable output-error state space model identification (MOESP) [11]. Both methods are regarded as subspace methods [12] for deriving a state-space model directly from input and output data. The Prony signal analysis method [13] and the time series model [14,15] have also been proposed during the last 30 years to identify modal parameters in various engineering fields.

Overspecifying the order of model is a popular approach among the time-domain methods for improving the accuracy of identified modal parameters from measured data with noise. This work concentrates on time series models to extract the modal parameters from measured input and output data. The high order auto-regressive (AR) and auto-regressive with exogeneous (ARX) models yield numerous of eigenvalues, only some of which belong to physical modes. Selecting physical modes and reducing the high order model to an equivalent physical model are key issues of the time-domain method.

Kumaresan and Tufts [16] presented a backward prediction model to determine the frequencies and damping factors from single-channel response data. Hollkamp and Batill [17] developed a single-input–single-output backward auto-regressive moving average (ARMA) model to predict the transient response of the sailplane subject to arbitrary inputs. Cooper [18] applied a backward prediction error model to extract the natural frequencies and damping factors from single-channel response data and indicated that the backward model has an advantage in separating physical modes from spurious modes. Hung and Ko [19] proposed the VBAR model to estimate the modal parameters and normal mode shapes from purely measured output data.

All the eigenvalues in the discrete-time domain estimated from a forward AR or ARX model by the least-square technique are always inside or on the unit circle in the z-plane. Therefore, the separation of system eigenvalues from spurious eigenvalues is difficult. In contrast, system eigenvalues computed by the backward model are outside or on the unit circle, and the spurious ones lie inside the unit circle. Accordingly, determining the system eigenvalues for the backward model is easier than for the forward model. When input information is absent, the modes induced from the input are unknown. Consequently, the determination of system modes using VBAR model is difficult. This paper proposes a VBARX model for selecting modes, deriving an equivalent state-space model and estimating modal parameters. The exogeneous (X) part implies that the computation of the VBARX model involves input excitation data. The VBARX model extends the applicability and increases the accuracy and practicability of the VBAR model when input data are available. The VBAR model can be regarded as a special case of the VBARX model in which the input part of the VBARX model is neglected.

2. Vector backward ARX model

The input and output relationship of a linear system can be described by a difference model. Given a measurement system with m outputs and r inputs, the difference equation for the input $u_t \in \Re^{r\times 1}$ and output $y_t \in \Re^{m\times 1}$ at discrete time t is

$$y_t = \sum_{i=1}^{q} a_i y_{t+i} + \sum_{j=0}^{q} b_j u_{t+j} + \varepsilon_t. \tag{1}$$

This difference model is called the VBARX (m, q, r) model. The subscript t is the discrete time index, and q is the order of the VBARX model. The matrices, $a_i \in \Re^{m\times m}$ and $b_j \in \Re^{m\times r}$, are the backward auto-regressive (BAR) parameter matrix and the backward exogeneous (BX) parameter matrix, respectively. $\varepsilon_t \in \Re^{m\times 1}$ is the prediction error. When the input is absent, such that $r = 0$, the VBARX (m, q, r) model reduces to a VBAR (m, q) model. If the number of time series data is N, then Eq. (1) can be expanded from time step $t = 1$ to $N - q$, and the following linear matrix equation is established:

$$\tilde{y}_q = P_q \tilde{Y}_q + \tilde{\varepsilon}_q, \tag{2}$$

where

$$P_q = [\, a_1 \quad \cdots \quad a_q \quad b_0 \quad b_1 \quad \cdots \quad b_q \,] \in \Re^{m\times(mq+r(q+1))}, \tag{3a}$$

$$\tilde{y}_q = [\, y_1 \quad y_2 \quad \cdots \quad y_{N-q} \,] \in \Re^{m\times(N-q)}, \tag{3b}$$

$$\tilde{Y}_q = \begin{bmatrix} y_2 & y_3 & \cdots & y_{N-q+1} \\ y_3 & y_4 & \cdots & y_{N-q+2} \\ \vdots & \vdots & \vdots & \vdots \\ y_{q+1} & y_{q+2} & \cdots & y_N \\ u_1 & u_2 & \cdots & u_{N-q} \\ u_2 & u_3 & \cdots & u_{N-q+1} \\ \vdots & \vdots & \vdots & \vdots \\ u_{q+1} & u_{q+2} & \cdots & u_N \end{bmatrix} \in \Re^{(mq+r(q+1))\times(N-q)}, \tag{3c}$$

$$\tilde{\varepsilon}_q = [\, \varepsilon_1 \quad \varepsilon_2 \quad \cdots \quad \varepsilon_{N-q} \,] \in \Re^{m\times(N-q)}. \tag{3d}$$

The BAR and the BX parameter matrices can be solved by the least-squares method.

A state vector consisting of output and input vectors of q-time steps is introduced as

$$\tilde{z}_t = \left\{ y_t^{\mathrm{T}} \quad y_{t+1}^{\mathrm{T}} \quad \cdots \quad y_{t+q-1}^{\mathrm{T}} \quad u_t^{\mathrm{T}} \quad u_{t+1}^{\mathrm{T}} \quad \cdots \quad u_{t+q-1}^{\mathrm{T}} \right\}^{\mathrm{T}} \in \Re^{(m+r)q\times 1}. \tag{4}$$

The following state-space equation is derived:

$$\tilde{z}_t = \tilde{A}\tilde{z}_{t+1} + \tilde{B}u_t, \tag{5}$$

where

$$\tilde{A} = \begin{bmatrix} \tilde{A}_{11} & \tilde{A}_{12} \\ 0 & \tilde{A}_{22} \end{bmatrix} \in \Re^{(m+r)q\times(m+r)q}, \quad \tilde{B} = \begin{bmatrix} \tilde{B}_1 \\ \tilde{B}_2 \end{bmatrix} \in \Re^{(m+r)q\times r} \tag{6a, b}$$

and

$$\tilde{A}_{11} = \begin{bmatrix} a_1 & a_2 & \cdots & a_{q-1} & a_q \\ I_m & 0 & \cdots & 0 & 0 \\ \vdots & \vdots & \vdots & \vdots & \vdots \\ 0 & 0 & \cdots & I_m & 0 \end{bmatrix} \in \Re^{mq\times mq}, \quad \tilde{A}_{12} = \begin{bmatrix} b_1 & b_2 & \cdots & b_q \\ 0 & 0 & \cdots & 0 \\ \vdots & \vdots & \vdots & \vdots \\ 0 & 0 & \cdots & 0 \end{bmatrix} \in \Re^{mq\times rq}, \tag{7a, b}$$

$$\tilde{A}_{22} = \begin{bmatrix} 0 & 0 & \cdots & 0 & 0 \\ I_r & 0 & \cdots & 0 & 0 \\ \vdots & \vdots & \vdots & \vdots & \vdots \\ 0 & 0 & \cdots & I_r & 0 \end{bmatrix} \in \Re^{rq\times rq}, \tag{7c}$$

$$\tilde{B}_1 = \begin{bmatrix} b_0 \\ 0 \\ \vdots \\ 0 \end{bmatrix} \in \Re^{mq\times r}, \quad \tilde{B}_2 = \begin{bmatrix} I_r \\ 0 \\ \vdots \\ 0 \end{bmatrix} \in \Re^{rq\times r}. \tag{8a, b}$$

The backward difference model specified by Eq. (1) can also be rewritten as follows:

$$y_t = \tilde{C}\tilde{z}_{t+1} + \tilde{D}u_t, \tag{9}$$

where

$$\tilde{C} = [\,a_1 \quad \cdots \quad a_q \; b_1 \quad \cdots \quad b_q\,] \in \Re^{m\times(m+r)q}, \quad \tilde{D} = b_0 \in \Re^{m\times r}. \tag{10a, b}$$

Eqs. (5) and (9) are the state equation and the output equation of the VBARX model, respectively. $\tilde{A}$, $\tilde{B}$, $\tilde{C}$ and $\tilde{D}$ are the discrete time backward state-space system matrix, input matrix, output matrix and transmission matrix, respectively.

The measurement noise disturbs the estimation of eigenvalues of the VBARX model when the signal-to-noise ratio (SNR) of the observed time series data is not sufficiently high. Overspecifying the order of model q is an effective method for increasing the accuracy of the eigenvalues estimated from noisy measurements. The number of vibration modes of a continuous structure is theoretically infinite. However, only the modes within the analysis frequency bandwidth, which depends on the sampling rate and the filtering passband of measured data, can be determined correctly. If the measured data for a structure contain n vibration modes, then the state equation includes n-pairs of conjugate system eigenvalues. The reduction of an equivalent state-space model then is obtained according to the following description, assuming that the system modes have been completely separated from the spurious modes.

A VBARX (m,q,r) model has $(m+r)q$ eigenvalues. Typically, $(m+r)q$ greatly exceeds $2n$, and the order of the VBARX model must be selected, such that $q \geqslant 2n/(m+r)$ to estimate accurately the modal parameters; otherwise, some system modes will be lost, and incorrect results may be

obtained. The polynomial of the backward state-space system is

$$p_b(\lambda) = \prod_{i=1}^{(m+r)q} (\lambda - \lambda_i) = \prod_{i=1}^{2n} (\lambda - \lambda_i) \prod_{i=2n+1}^{(m+r)q} (\lambda - \lambda_i) = 0. \tag{11}$$

The total of $(m+r)q$ eigenvalues include $2n$ system eigenvalues and $(m+r)q-2n$ spurious eigenvalues. The spurious modes should be removed, and the system modes should be retained to establish the physical state equation of motion to determine the modal parameters. Kumaresan and Tufts [16] stated that the magnitudes of the eigenvalues of the backward model are:

$$|\lambda_i| \geqslant 1.0 \quad \text{for } i \leqslant 2n, \quad \text{and} \quad |\lambda_i| < 1.0 \quad \text{for } i > 2n. \tag{12}$$

For the backward model, the first $2n$ eigenvalues outside or on the unit circle at the origin in the z-plane are attributed to the system modes, and the remaining $(m+r)q-2n$ eigenvalues are the spurious modes. The state equation derived from the proposed VBARX model provides a determinate boundary between the system modes and the spurious modes.

The backward state-space system matrix $\tilde{A}$ can be decomposed into eigenvector matrix Ψ and diagonal eigenvalue matrix Λ. According to Eqs. (11) and (12), the matrices Ψ and Λ can be partitioned into sub-matrices as follows [19]:

$$\tilde{A} = \Psi \Lambda \Psi^{-1} = \begin{bmatrix} \Psi_{ss} & \Psi_{sn} \\ \Psi_{ns} & \Psi_{nn} \end{bmatrix} \begin{bmatrix} \Lambda_s & 0 \\ 0 & \Lambda_n \end{bmatrix} \begin{bmatrix} \Psi_{ss} & \Psi_{sn} \\ \Psi_{ns} & \Psi_{nn} \end{bmatrix}^{-1}, \tag{13}$$

where the subscripts "s" and "n" indicate "system" modes and "spurious" modes, respectively. Λ_s and Λ_n are the diagonal sub-matrices that contain the $2n$ system eigenvalues and $(m+r)q-2n$ spurious eigenvalues, respectively. The matrices $\tilde{B}$, $\Psi^{-1}\tilde{B}$ and $\tilde{C}$ are also partitioned as

$$\tilde{B} = \begin{bmatrix} \tilde{B}_s \\ \tilde{B}_n \end{bmatrix}, \quad \Psi^{-1}\tilde{B} = \begin{bmatrix} B_s \\ B_n \end{bmatrix}, \tag{14a, b}$$

$$\tilde{C} = [\, \tilde{C}_s \quad \tilde{C}_n \,]. \tag{15}$$

From Eqs. (13) to (15), a reduced order backward state-space model in the form of Eqs. (5) and (9) can be constructed by removing the corresponding columns and rows of $(m+r)q-2n$ spurious modes, as follow:

$$A'_d = \Psi_{ss} \Lambda_s \Psi_{ss}^{-1}, \quad B'_d = \Psi_{ss} B_s, \tag{16a, b}$$

$$C'_d = \tilde{C}_s + \tilde{C}_n \Lambda_{ns} \Psi_{ss}^{-1}, \quad D'_d = \tilde{D}, \tag{16c, d}$$

where $A'_d \in \Re^{2n \times 2n}$, $B'_d \in \Re^{2n \times r}$, $C'_d \in \Re^{m \times 2n}$ and $D'_d \in \Re^{m \times r}$ are the reduced state system matrix, the input matrix, the output matrix and the transmission matrix, respectively.

The reduced order backward state-space model in discrete time represented by (A'_d, B'_d, C'_d, D'_d) can be transformed into the forward model (A_d, B_d, C_d, D_d). The relationships between the forward and backward state-space matrices are [19]:

$$A_d = A'^{-1}_d, \quad B_d = -A'^{-1}_d B'_d, \tag{17a, b}$$

$$C_d = C'_d A'^{-1}_d, \quad D_d = D'_d - C'_d A'^{-1}_d B'_d. \tag{17c, d}$$

Then, the reduced order state-space model in discrete time, (A_d, B_d, C_d, D_d), can be transformed into a continuous time model, represented by (A_c, B_c, C_c, D_c), as follows [20]:

$$A_c = \ln(A_d)/\Delta t, \quad B_c = A_c(A_d - I)B_d, \tag{18a, b}$$

$$C_c = C_d, \quad D_c = D_d. \tag{18c, d}$$

3. Extraction of modal parameters

The equation of motion for a structural system with n d.o.f.s is expressed as

$$M\ddot{x}(t) + E\dot{x}(t) + Kx(t) = B_0u(t), \tag{19}$$

where t is the continuous time; $x(t) \in \Re^{n\times 1}$ is the displacement vector; $u(t) \in \Re^{r\times 1}$ is the force vector; $M \in \Re^{n\times n}$ is a positive-definite mass matrix; $E \in \Re^{n\times n}$ is a positive-semidefinite damping matrix; $K \in \Re^{n\times n}$ is a positive-semidefinite stiffness matrix, and $B_0 \in \Re^{n\times r}$ is the input influence matrix. The dots denote differentiation with respect to time. Not all of the d.o.f.s are observed in the practical experimental identification of the dynamic characteristics of structures. Moreover, the sensors of displacement, velocity, and acceleration may be arranged at different locations to measure simultaneously the different types of dynamic response. For a measurement system with m output sensors on structures, the output equation of the structural system for combined displacement, velocity and acceleration (DVA) measurements is expressed as [20]

$$y(t) = c_a\ddot{x}(t) + c_v\dot{x}(t) + c_dx(t), \tag{20}$$

where $y(t) \in \Re^{m\times 1}$ is the output vector; c_d, c_v and $c_a \in \Re^{m\times n}$ are the output influence matrices of displacement, velocity and acceleration, respectively. After the state vector,

$$z(t) = \begin{bmatrix} x(t) \\ \dot{x}(t) \end{bmatrix} \in \Re^{2n\times 1}, \tag{21}$$

is introduced, the equations of motion for the physical model described by Eq. (19) can be transformed into the following state equation of motion:

$$\dot{z}(t) = Az(t) + Bu(t), \tag{22}$$

where

$$A = \begin{bmatrix} 0_n & I_n \\ -M^{-1}K & -M^{-1}E \end{bmatrix}, \quad B = \begin{bmatrix} 0_{n\times r} \\ M^{-1}B_0 \end{bmatrix}. \tag{23a, b}$$

$A \in \Re^{2n\times 2n}$ and $B \in \Re^{2n\times r}$ are the system matrix and the input matrix, respectively. The output equation, Eq. (20), can be transformed as,

$$y(t) = Cz(t) + Du(t), \tag{24}$$

where

$$C = [\, c_d - c_aM^{-1}K \quad c_v - c_aM^{-1}E \,], \quad D = c_aM^{-1}B_0. \tag{25a, b}$$

Here, $C \in \Re^{m\times 2n}$ is the output matrix of the state vector $z(t)$, and $D \in \Re^{m\times r}$ is the direct transmission matrix. The matrix D will disappear from Eq. (24) when acceleration is not a measured output.

The natural frequencies and damping ratios can be determined by an eigenanalysis of the system matrix A in Eq. (23a). The eigenanalysis of the identified equivalent system matrix A_c in Eq. (18a) should provide corresponding results for a noise-free system. The natural frequencies and damping ratios in terms of the eigenvalues ($s_i = \alpha_i + j\beta_i$, $i = 1, 2, ..., n$) of A or A_c are,

$$\omega_i = \sqrt{\alpha_i^2 + \beta_i^2} \quad \text{and} \quad \xi_i = -\alpha_i/\omega_i, \quad i = 1, 2, ..., n. \tag{26a, b}$$

The normal mode shapes are the eigenvectors of matrix $M^{-1}K$, which appears as the left-lower block of matrix A. Although the identified system matrix A_c has the same modal parameters as matrix A, the distributions of the elements in these two matrices are different. Therefore, the normal modes cannot be directly determined from the left-lower block of matrix A_c. Hung et al. [21] presented a transformation matrix T for transforming the identified system matrix A_c into a matrix of the same type as matrix A. The transformation matrix can be expressed in terms of the identified matrices A_c and C_c, and the output influence matrices for displacement, velocity and acceleration, as follows:

$$T = \begin{bmatrix} T_1 \\ T_2 \end{bmatrix}, \tag{27}$$

where

$$T_1 = c_d C_c + c_v C_c A_c^{-1} + c_a C_c A_c^{-2}, \quad T_2 = T_1 A_c. \tag{28a, b}$$

When only one of the displacement, velocity and acceleration is available to be measured, the transformation matrices are:

$$T_d = \begin{bmatrix} C_c \\ C_c A_c \end{bmatrix} \quad \text{for displacement only,} \tag{29a}$$

$$T_v = T_d A_c^{-1} = \begin{bmatrix} C_c A_c^{-1} \\ C_c \end{bmatrix} \quad \text{for velocity only,} \tag{29b}$$

$$T_a = T_d A_c^{-2} = \begin{bmatrix} C_c A_c^{-2} \\ C_c A_c^{-1} \end{bmatrix} \quad \text{for acceleration only.} \tag{29c}$$

The transformed system matrix $\bar{A}$ of the same type as physical system matrix A in Eq. (23a) can be obtained by the following transformation:

$$\bar{A} = T A_c T^{-1}. \tag{30}$$

The normal mode shapes are the eigenvectors of the negative sub-matrix, which is the left-lower block of matrix $\bar{A}$.

4. Numerical examples

A lumped mass model with 3 d.o.f.s [22], shown in Fig. 1 is selected as a case study to illustrate the availability of the proposed VBARX approach. The parameters of this model are $m_1 = 1$, $m_2 = 2$, $m_3 = 3$, $c_1 = c_4 = c_5 = 0.1$, $c_2 = c_3 = 0.2$, $k_1 = 10$, $k_2 = 20$ and $k_3 = 30$. The system is excited at m_3, and the time–history responses of displacement, velocity and acceleration, are picked at m_1, m_2 and m_3, respectively. The fourth order Runge–Kutta method is employed to calculate the dynamic responses in the numerical examples. The sampling rate of the time series data is 5 Hz, and the length of the recorded data is selected as only 256 points to test whether the VBARX model can be applied to short-recorded data. Table 1 shows the true values of natural frequencies and damping ratios of the model with 3 d.o.f.s.

The numerical examples cover four different types of inputs; (1) single sinusoidal input with an exciting frequency of 0.4 Hz; (2) sinusoidal input at ten different frequencies; (3) zero-mean white noise input, and (4) combined input. The VBAR model without an input force is considered for comparison to demonstrate the advantage of the proposed method under forced vibration in Cases 1–3. Table 2 compares the identified natural frequencies, damping ratios and modal

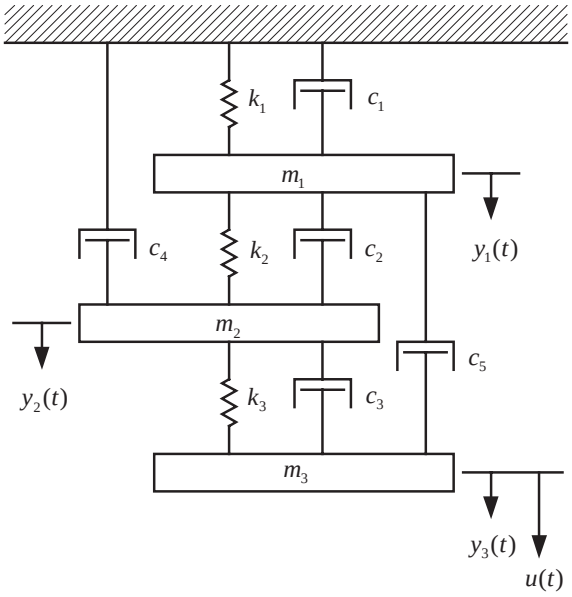

Fig. 1. 3-d.o.f. lumped mass model.

Table 1
Exact natural frequencies and damping ratios of the 3-d.o.f model

Mode	Natural frequency, ω_i (Hz)	Damping ratio, ξ_i (%)
1	0.1699	1.7626
2	0.7120	3.4783
3	1.0537	3.7849

Table 2
Comparison of identified natural frequencies, damping ratios and MAC values with various types of input

	Mode	Natural frequency, ω_i (Hz)	Damping ratio, ξ_i (%)	MAC
(a) Case 1: Single sinusoidal input (0.4 Hz) under noise-free condition				
VBARX (3,5,1)	1	0.1699	1.7626	1.0000
	2	0.7120	3.4783	1.0000
	3	1.0537	3.7849	1.0000
VBAR (3,10)	1	0.1699	1.7626	1.0000
		0.4000	**0.0000**	
	2	0.7120	3.4783	1.0000
	3	1.0537	3.7849	1.0000
(b) Case 2: Multiple sinusoidal input (0.1, 0.4, 0.7, 1.0, 1.3, 1.6, 1.9, 2.2, 2.5, 2.8 Hz) under noise-free condition				
VBARX (3,5,1)	1	0.1699	1.7626	1.0000
	2	0.7120	3.4783	1.0000
	3	1.0537	3.7849	1.0000
VBAR (3,20)		**0.1003**	**−0.4524**	
	1	0.1697	2.0584	1.0000
		0.4000	**−0.0156**	
	2	0.7120	3.4789	1.0000
		1.0002	**0.0008**	
	3	1.0536	3.7864	1.0000
		1.2999	**0.0003**	
		1.6000	**−0.0005**	
		1.9000	**0.0001**	
		2.2000	**−0.0001**	
(c) Case 3: White noise type input under noise-free condition				
VBARX (3,5,1)	1	0.1699	1.7626	1.0000
	2	0.7120	3.4783	1.0000
	3	1.0537	3.7849	1.0000
VBAR (3,55)		**0.1582**	**0.6402**	
		0.5396	**2.5293**	
		0.6588	**0.3509**	
		0.7039	**0.5666**	
		0.7750	**0.2490**	
		0.8920	**0.5423**	
		1.0397	**0.1213**	
		1.3148	**0.5058**	
		1.4762	**0.2008**	
		2.2237	**0.1283**	

assurance criteria (MAC) [23] obtained by the proposed approach with those obtained by the VBAR model under noise-free conditions in Cases 1–3. The MAC is an approximate index of the accuracy of the identified mode shape.

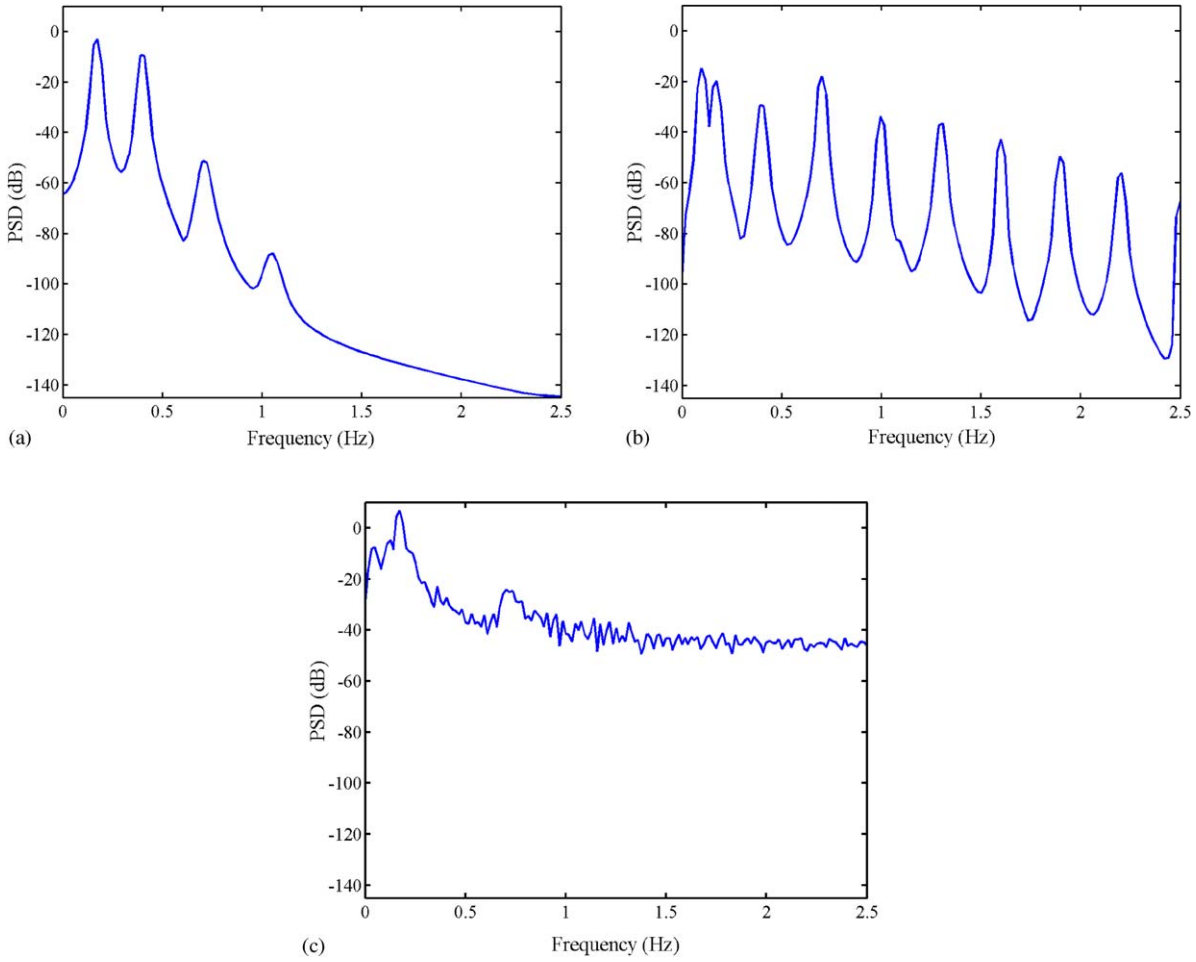

Fig. 2. PSD of response at m_3 of the 3-d.o.f. lumped mass model. (a) Case 1: Sinusoidal input with a single frequency; (b) Case 2: sinusoidal input with ten various frequencies; (c) Case 3: zero-mean white noise input.

Fig. 2(a) shows the power spectrum density (PSD) of the output displacement response at m_3 in Case 1. The right-sided part of Fig. 3(a) indicates 30 eigenvalues for the VBAR (3,10) model, of which eight are on or outside the unit circle. Input information is lacking so the VBAR model cannot distinguish which two eigenvalues are associated with the input-induced mode. Thus, the VBAR model yields four modes, as shown in Table 2(a). However, the VBARX model clearly distinguishes the six system eigenvalues, as indicated in the left-sided part of Fig. 3(a) and Table 2(a). The VBARX (3,5,1) model has 20 eigenvalues, of which five are located exactly in the origin of the unit circle in this case. Therefore, it seems that only 16 eigenvalues are shown in the left-sided part of Fig. 3(a). The input-induced mode, as estimated by the VBAR model, can be manually identified with knowledge of the damping ratio, which is in fact zero. Nevertheless, when the input includes multi-harmonic components, the estimation of the actual damping ratios is difficult.

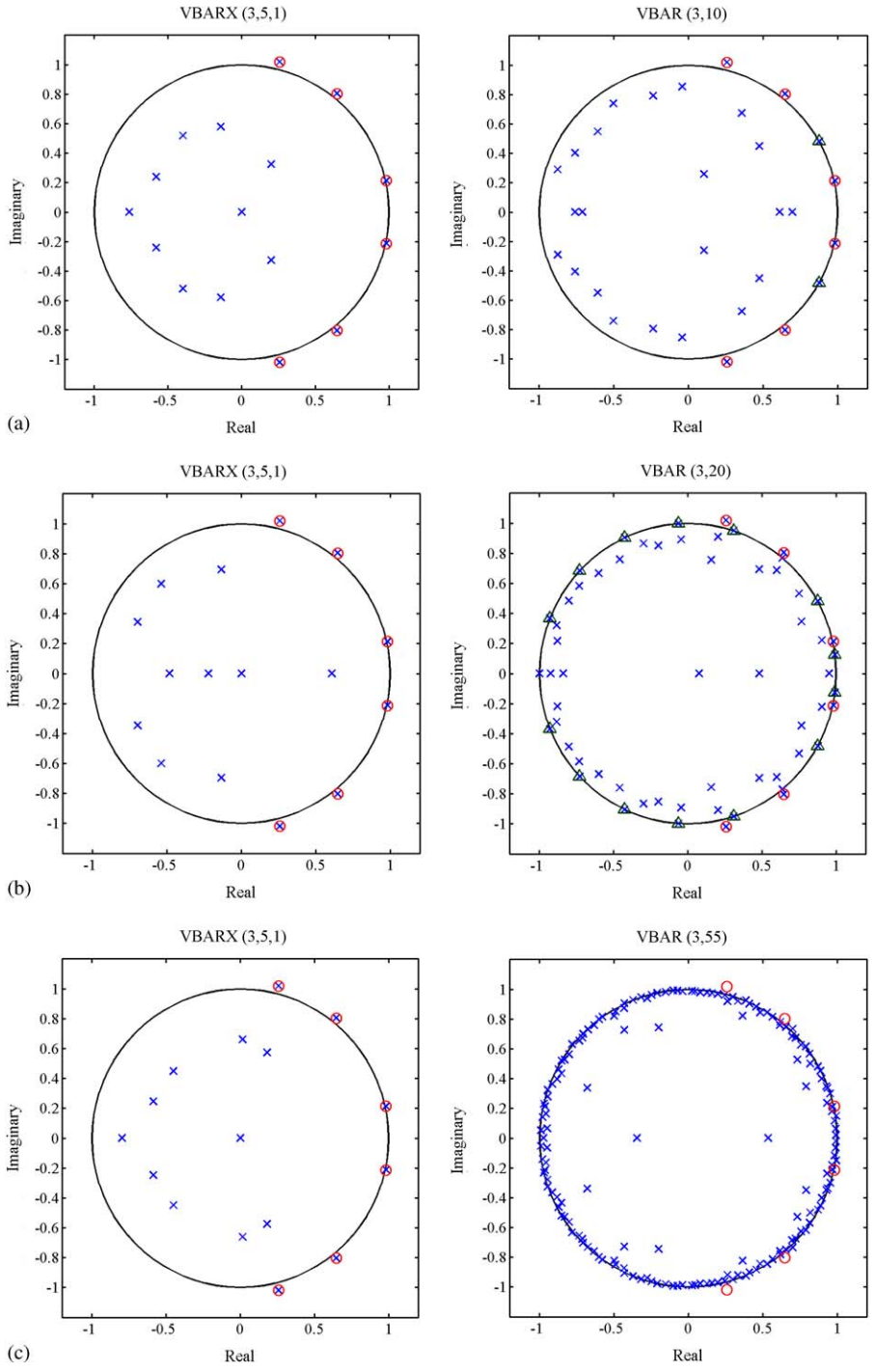

Fig. 3. Eigenvalue distributions of VBARX and VBAR models. (a) Case 1; (b) Case 2; (c) Case 3; ○, true eigenvalue; ×, eigenvalue before discrimination; △, eigenvalue induced by input.

In Case 2, sinusoidal data of ten different frequencies, 0.1, 0.4, 0.7, 1.0, 1.3, 1.6, 1.9, 2.2, 2.5 and 2.8 Hz, are combined to generate the input data, and all data are noise-free. Fig. 2(b) shows the PSD of the output displacement response at m_3. Because the sampling rate is 5 Hz and the Nyquist frequency [24] is 2.5 Hz, the last harmonic component with a frequency 2.8 Hz is not sampled adequately. Table 2(b) and Fig. 3(b) indicate that the VBARX model can also yield correctly system modes when the input data have multi-harmonic components. However, the VBAR model yields several spurious modes induced by input data.

In Case 3, the input data are white noise type of force with zero mean, and all data are noise-free. Fig. 2(c) shows the PSD of the output displacement response at m_3. Table 2(c) and Fig. 3(c) indicate that the VBARX model can still yield exact system modes with white noise input. In the case of white noise excitation with short-recorded data, the VBAR model cannot distinguish the system modes from the input-induced modes. Additionally, Table 2(c) shows that the damping ratios identified by the VBAR model are not zero. Therefore, the input-induced modes should be manually identified using further information.

The VBARX model can yield accurate results with smaller order than the VBAR model, and it can also automatically identify modal parameters without other auxiliaries for selecting system modes in Cases 1–3. Case 4 is used to examine the accuracy of only the VBARX model. The input data in Cases 2 and 3 were combined to excite the system at m_3. Fig. 4 shows the PSD of the displacement response at m_3. Zero-mean white noise with an r.m.s. of 10%, 20% and 30% of the measured response was added to the noise-free response data to simulate measurement noise. Table 3 lists identified natural frequencies, damping ratios and MAC values with combined input at various noise levels in Case 4. It indicates that the VBARX model can yield quite accurate results when noise levels are below 30%. Case 4 also shows that the order of the VBARX model will be increased when measured data are contaminated by more noise. The selection of order for the VBARX model and other identification methods is a beginning but important step in a complete identification procedure. If the order chosen is too small, some of weaker modes cannot be identified. In contrast, if the order is too large, it not only costs too much, but also generates

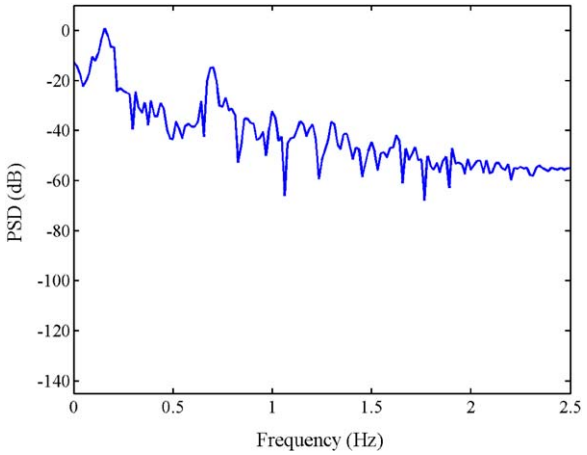

Fig. 4. PSD of response at m_3 of the 3-d.o.f. lumped mass model in Case 4.

Table 3
Case 4: Identified natural frequencies, damping ratios and MAC values with combined input at various noise levels

	Mode	Natural frequency, ω_i (Hz)	Damping ratio, ξ_i (%)	MAC
Noise-free	1	0.1699	1.7626	1.0000
VBARX (3,5,1)	2	0.7120	3.4783	1.0000
	3	1.0537	3.7849	1.0000
10% noise	1	0.1688	1.6855	1.0000
VBARX (3,10,1)	2	0.7108	3.2921	0.9978
	3	1.0541	3.1578	0.9988
20% noise	1	0.1682	1.3781	0.9997
VBARX (3,20,1)	2	0.7096	2.6812	0.9999
	3	1.0451	2.4406	0.9950
30% noise	1	0.1726	1.1673	0.9966
VBARX (3,35,1)	2	0.7172	2.1641	0.9906
	3	1.0596	2.3064	0.9547

too many spurious modes. The definite steps to choose order for the proposed VBARX model are still developing. In addition, an experienced user may select the order better.

5. Experimental example and discussion

A benchmark model established by NCREE in Taiwan [25] is used as an experimental model to test the proposed VBARX approach can be applied to real-world structures. This benchmark model is a five-story $\frac{1}{2}$-scale steel frame with dimensions of $3 \times 2\,m^2$ in-plane and 1.3 m height for each story. Fig. 5 depicts the top view and the side view of the frame structure, and Table 4 presents the natural frequencies determined by Loh et al. [26]. The first and second modes in the X and Y directions are represented by $X1$, $X2$, $Y1$ and $Y2$. The experimental data are seismic responses generated through a shaking table test. Furthermore, the seismic records of ground acceleration in the El. Centro and Kobe earthquakes were taken as the accelerations of the shaking table. Kobe XY 8% implies that the loading acceleration is 8% in both the X- and Y directions of that of the Kobe earthquake; El. Centro XY 20%30% indicates that the loading acceleration is 20% in X direction and 30% in Y direction of that of the El. Centro earthquake.

Fig. 6 presents the orientations and positions of the accelerometers on the benchmark model. A3–A12 (X direction) and A15, A17, A19, A21 and A23 (Y direction) are selected as output channels; A1, A2 and A13 are selected as input channels. Fig. 7 shows the time–history and the PSD of the accelerations measured at A1 in the X direction under both seismic accelerations. The sampling rate of the original data series is 200 Hz, and the number of data is approximately 6000 points. Only 2048 data points in Fig. 8 were selected in this example. The original data were firstly fed into a 50 Hz anti-aliasing low pass filter, and then the filtered data were resampled the at a

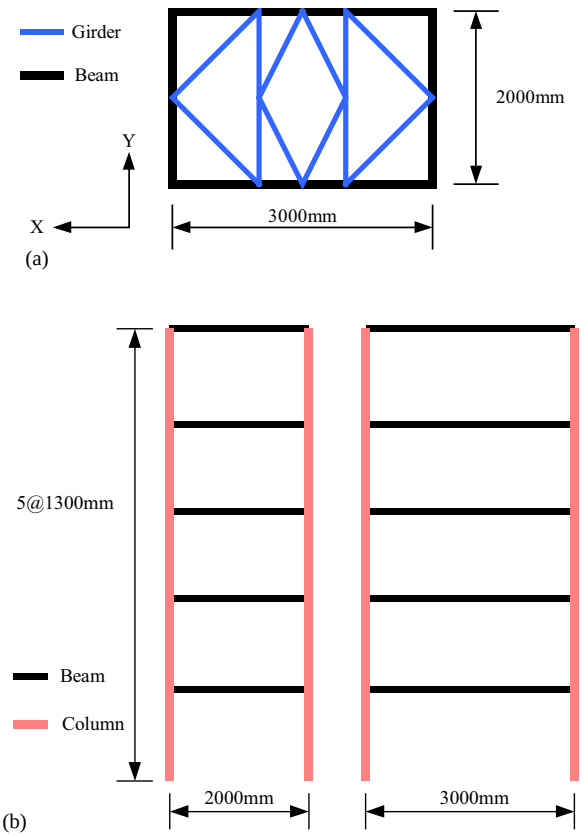

Fig. 5. (a) Top view of frame structure and (b) side view of frame structure.

Table 4
Natural frequencies of frame structure [26]

Mode	Natural frequency (Hz)
$X1$	1.4306
$Y1$	2.1413
$X2$	4.6296
$Y2$	6.9930

sampling rate of 100 Hz. Consequently, a total of 1024 data points per channel were used in this experimental analysis.

Table 5 lists 15 natural frequencies and damping ratios identified by the VBARX model in the Kobe XY 8% and El. Centro XY 20%30% cases. Here, Ti refers to the ith torsion mode. The natural frequencies in the two seismic cases agree closely with each other. The variances of the identified damping ratios are much higher than those of the identified natural frequencies, according to the stochastic characteristics and non-linearity of the measured data. Tables 6 and 7 list the first 15 normal mode shapes in X, Y and T directions in both seismic cases. Tables 5–7

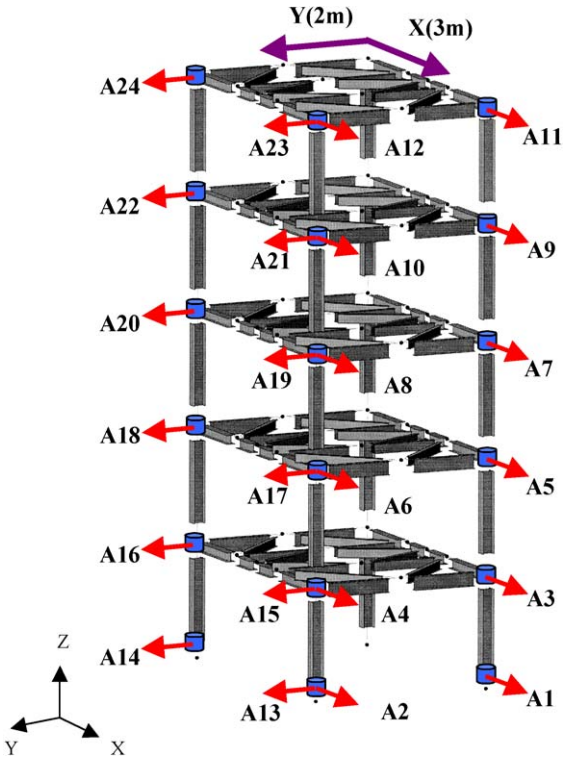

Fig. 6. Orientation and position of accelerometers on frame model [25].

show that the VBARX model can identify not only the natural frequencies and the damping ratios, but also the normal mode shapes. Fig. 9 shows some of the normal mode shapes described in Tables 6 and 7. These normal mode shapes are similar between the two seismic cases. The identified results can be compared with literatures [21,26].

6. Conclusion

This work proposes a VBARX model, which is an extension of VBAR model, to identify the modal parameters of structures using measured input and output data. This method not only accurately determines the natural frequency and damping ratio, but also effectively extracts the normal mode shapes. The main advantage of this proposed VBARX approach is that the system eigenvalues can be clearly separated from the spurious modes by the boundary of the unit circle.

When the measured data do not concern free responses but the forced responses, the VBAR model without input excitation cannot easily separate the system modes from input-induced modes. In contrast, the proposed VBARX model can easily determine the true order of system modes, separate them from the spurious modes and derive the equivalent system. The results of both numerical and experimental examples indicate that the VBARX model determines the system modes more efficiently than the VBAR model. Both the VBAR model and the VBARX

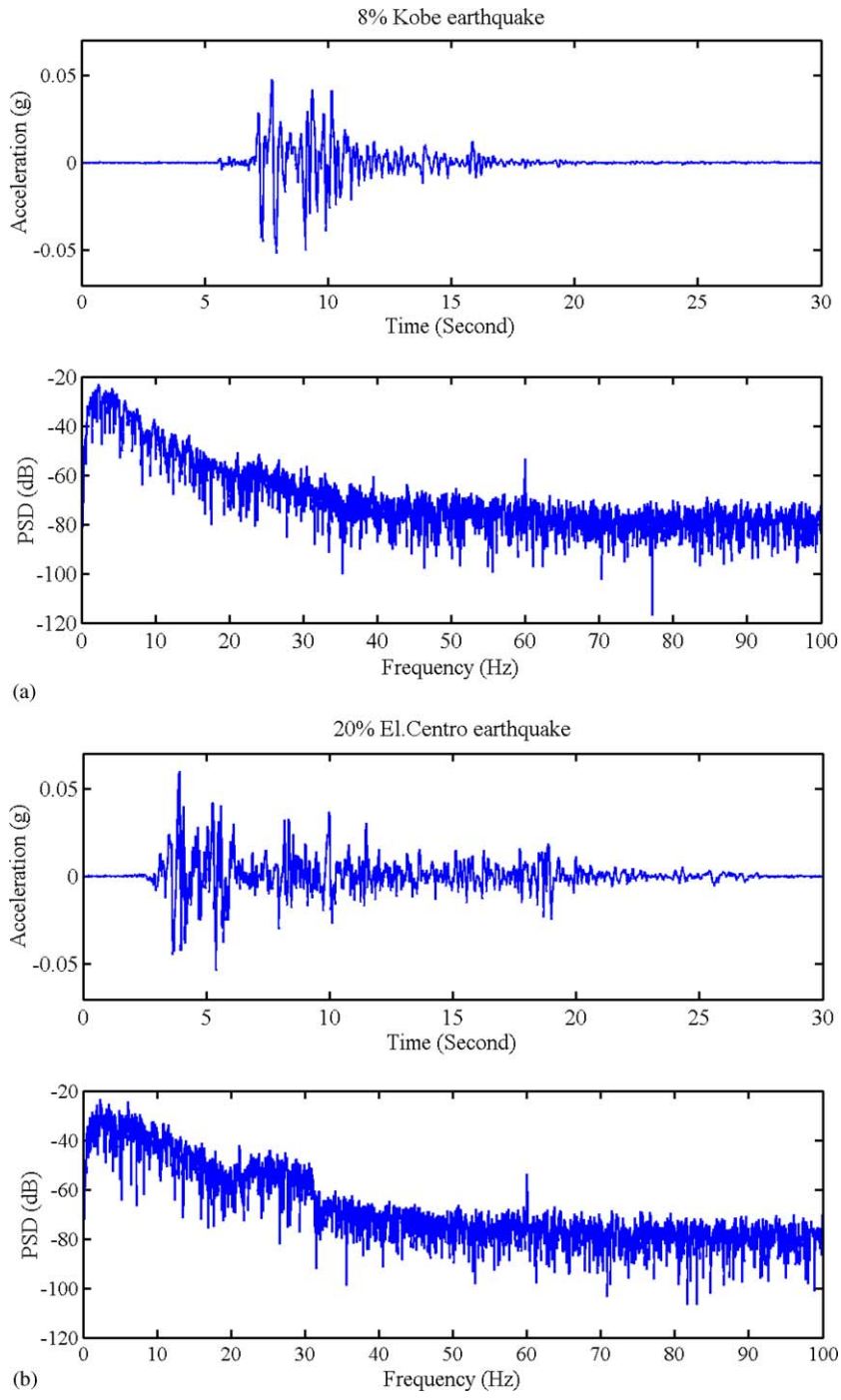

Fig. 7. (a) Time–history and PSD of 8% Kobe earthquake input acceleration. (b) Time–history and PSD of 20% El. Centro earthquake input acceleration.

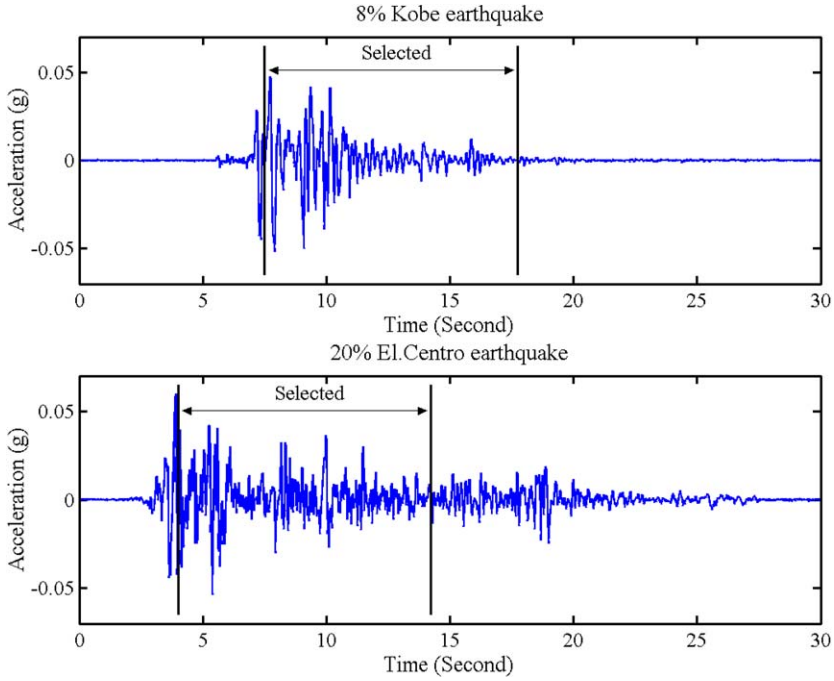

Fig. 8. Selected periods of 8% Kobe and 20% El. Centro earthquakes.

Table 5
Comparison of natural frequencies and damping ratios identified by VBARX (15,30,3) model in Kobe XY 8% and El. Centro XY 20%30% cases

Mode No.	Kobe XY 8% case		El. Centro XY 20%30% case	
	Natural frequency, ω_i (Hz)	Damping ratio, ξ_i (%)	Natural frequency, ω_i (Hz)	Damping ratio, ξ_i (%)
1 ($X1$)	1.4055	0.9004	1.3928	1.6106
2 ($Y1$)	2.0822	2.0673	2.0815	3.0574
3 ($T1$)	3.5321	0.3862	3.5402	0.4436
4 ($X2$)	4.5335	0.1663	4.5503	0.2820
5 ($Y2$)	6.8932	0.0963	6.9198	1.3420
6 ($X3$)	8.2139	0.1734	8.2332	0.6265
7 ($T2$)	11.4386	0.3196	11.3874	5.3293
8 ($X4$)	12.3785	0.3396	12.3719	0.0264
9 ($Y3$)	12.6858	0.2129	12.6421	0.3351
10 ($X5$)	16.0047	0.1486	15.9997	0.1034
11 ($Y4$)	18.2491	0.7647	18.3444	0.8313
12 ($T3$)	21.2541	0.1553	21.2410	0.2800
13 ($Y5$)	25.2142	0.0690	25.1311	0.1507
14 ($T4$)	32.1251	0.1567	32.1913	0.2306
15 ($T5$)	40.5410	0.0522	40.2912	0.4694

Table 6

Position	Mode (Hz)							
	1 ($X1$)	2 ($Y1$)	3 ($T1$)	4 ($X2$)	5 ($Y2$)	6 ($X3$)	7 ($T2$)	8 ($X4$)
	1.4055	2.0822	3.5321	4.5335	6.8932	8.2139	11.4386	12.3785
(a) Normal mode shapes determined by VBARX (15,30,3) model in Kobe XY 8% case (Mode 1–8)								
A3	0.0857	−0.0011	−0.0506	−0.2501	0.0033	0.3928	0.1660	0.4244
A5	0.2085	0.0001	−0.1307	−0.4366	0.0044	0.2517	0.3100	−0.2095
A7	0.3004	0.0030	−0.2025	−0.2840	0.0013	−0.3058	0.2098	−0.2125
A9	0.3952	0.0045	−0.2722	0.0650	−0.0017	−0.3044	−0.0323	0.4040
A11	0.4424	−0.0083	−0.3039	0.4032	0.0072	0.3044	−0.2813	−0.1726
A4	0.0874	0.0013	0.0543	−0.2494	0.0072	0.3894	−0.1607	0.4245
A6	0.2132	−0.0020	0.1308	−0.4195	−0.0102	0.2415	−0.2893	−0.2064
A8	0.3151	0.0034	0.2124	−0.3005	−0.0010	−0.3223	−0.2145	−0.2175
A10	0.3956	0.0000	0.2723	0.0668	−0.0012	−0.3026	0.0292	0.3993
A12	0.4429	0.0094	0.2954	0.4076	−0.0057	0.3128	0.2608	−0.1904
A15	−0.0126	0.1193	0.0726	0.0150	0.3386	−0.0128	−0.3266	−0.1522
A17	−0.0137	0.2844	0.2026	0.0062	0.6036	−0.0042	−0.4713	−0.0749
A19	−0.0197	0.4391	0.3210	0.0043	0.4391	0.0038	−0.2473	0.1252
A21	−0.0243	0.5557	0.4147	−0.0034	−0.0640	0.0065	0.1058	0.1077
A23	−0.0271	0.6349	0.4744	−0.0079	−0.5691	0.0013	0.3558	−0.1263

(b) Normal mode shapes determined by VBARX (15,30,3) model in Kobe XY 8% case (Mode 9–15)

	9 ($Y3$)	10 ($X5$)	11 ($Y4$)	12 ($T3$)	13 ($Y5$)	14 ($T4$)	15 ($T5$)
	12.6858	16.0047	18.2491	21.2541	25.2142	32.1251	40.5410
A3	0.0074	−0.3153	−0.0944	0.2735	−0.0520	0.3211	0.2632
A5	0.0119	0.4121	0.0557	0.1892	−0.0220	−0.1398	−0.3286
A7	0.0116	−0.3696	−0.0213	−0.2045	−0.0293	−0.1693	0.2958
A9	0.0015	0.2756	−0.0063	−0.2222	0.0008	0.3061	−0.1897
A11	−0.0258	−0.0916	−0.0334	0.2120	−0.0604	−0.1166	0.0734
A4	0.0049	−0.3152	0.1017	−0.2622	0.0152	−0.3163	−0.2445
A6	−0.0117	0.4079	−0.0846	−0.1842	0.0104	0.1317	0.3040
A8	−0.0201	−0.3966	0.0562	0.2112	−0.0261	0.1892	−0.2862
A10	0.0005	0.2769	−0.0109	0.2216	−0.0530	−0.3045	0.1705
A12	0.0240	−0.0993	0.0407	−0.2167	0.0588	0.1327	−0.0570
A15	0.5414	−0.0015	0.7245	−0.3581	−0.4695	−0.4224	−0.3091
A17	0.3332	−0.0003	−0.3809	−0.2746	0.5922	0.1922	0.4015
A19	−0.4615	0.0047	−0.1872	0.2942	−0.5534	0.2430	−0.3600
A21	−0.4334	−0.0004	0.3754	0.3395	0.3029	−0.4107	0.2024
A23	0.4391	−0.0089	−0.3434	−0.3232	−0.1259	0.1866	−0.0097

Table 7

Position	Mode (Hz)							
	1 ($X1$)	2 ($Y1$)	3 ($T1$)	4 ($X2$)	5 ($Y2$)	6 ($X3$)	7 ($T2$)	8 ($X4$)
	1.3928	2.0815	3.5402	4.5503	6.9198	8.2332	11.3874	12.3719
(a)Normal mode shapes determined by VBARX (15,30,3) model in El. Centro XY 20%30% case (Mode 1–8)								
A3	0.0890	−0.0011	−0.0477	−0.2463	0.0014	0.3865	0.1479	0.4225
A5	0.2151	−0.0043	−0.1123	−0.4343	0.0015	0.2684	0.1828	−0.2201
A7	0.2974	0.0022	−0.1798	−0.2707	0.0004	−0.2863	0.1312	−0.2216
A9	0.3982	0.0039	−0.2430	0.0677	−0.0028	−0.2934	0.0248	0.4283
A11	0.4452	−0.0092	−0.2647	0.4008	0.0083	0.3039	−0.1391	−0.1761
A4	0.0891	0.0009	0.0439	−0.2455	0.0057	0.3712	−0.0496	0.4435
A6	0.2113	−0.0018	0.1174	−0.4307	−0.0033	0.2337	−0.2251	−0.1929
A8	0.3128	0.0015	0.1847	−0.2958	−0.0014	−0.3193	−0.1466	−0.2205
A10	0.3914	−0.0025	0.2428	0.0699	−0.0017	−0.2899	−0.0056	0.4280
A12	0.4394	0.0073	0.2784	0.4057	−0.0068	0.3103	0.1976	−0.2059
A15	0.0046	0.1151	0.0548	0.0610	0.3357	−0.0032	0.2356	0.0060
A17	0.0177	0.2811	0.2006	0.0388	0.6047	−0.1138	−0.3290	0.0266
A19	0.0250	0.4363	0.3443	0.0073	0.4385	−0.1170	−0.4964	0.0121
A21	0.0371	0.5566	0.4498	−0.0312	−0.0651	−0.0136	−0.0837	−0.0161
A23	0.0402	0.6383	0.5228	−0.0567	−0.5700	0.1290	0.6137	−0.0136

(b) Normal mode shapes determined by VBARX (15,30,3) model in El. Centro XY 20%30% case (Mode 9–15)

	9 ($Y3$)	10 ($X5$)	11 ($Y4$)	12 ($T3$)	13 ($Y5$)	14 ($T4$)	15 ($T5$)
	12.6421	15.9997	18.3444	21.2410	25.1311	32.1913	40.2912
A3	−0.0037	−0.3146	−0.0849	0.2345	−0.0113	0.3219	0.2680
A5	0.0166	0.4102	0.1041	0.2433	0.0116	−0.1801	−0.3686
A7	0.0150	−0.3675	−0.0285	−0.2125	−0.0179	−0.1534	0.2587
A9	−0.0053	0.2759	−0.0195	−0.2271	0.0007	0.2856	−0.1552
A11	−0.0203	−0.0845	−0.0202	0.2193	−0.0137	−0.0882	0.0253
A4	−0.0059	−0.3150	0.1016	−0.2077	−0.0071	−0.3431	−0.3005
A6	−0.0115	0.4148	−0.1275	−0.2435	−0.0065	0.1667	0.3325
A8	−0.0142	−0.3990	0.0733	0.2312	0.0020	0.1597	−0.2725
A10	−0.0059	0.2735	−0.0068	0.2229	−0.0217	−0.2807	0.1123
A12	0.0262	−0.0934	−0.0048	−0.2275	0.0010	0.0996	−0.0885
A15	0.5492	0.0018	0.7741	−0.3734	−0.5056	−0.4842	−0.2932
A17	0.3159	0.0141	−0.3384	−0.2647	0.5867	0.2276	0.4049
A19	−0.4645	0.0001	−0.1953	0.3759	−0.5437	0.2192	−0.3488
A21	−0.4247	−0.0123	0.3847	0.2483	0.3168	−0.3540	0.1810
A23	0.4477	−0.0010	−0.2202	−0.2670	−0.0545	0.1782	0.0282

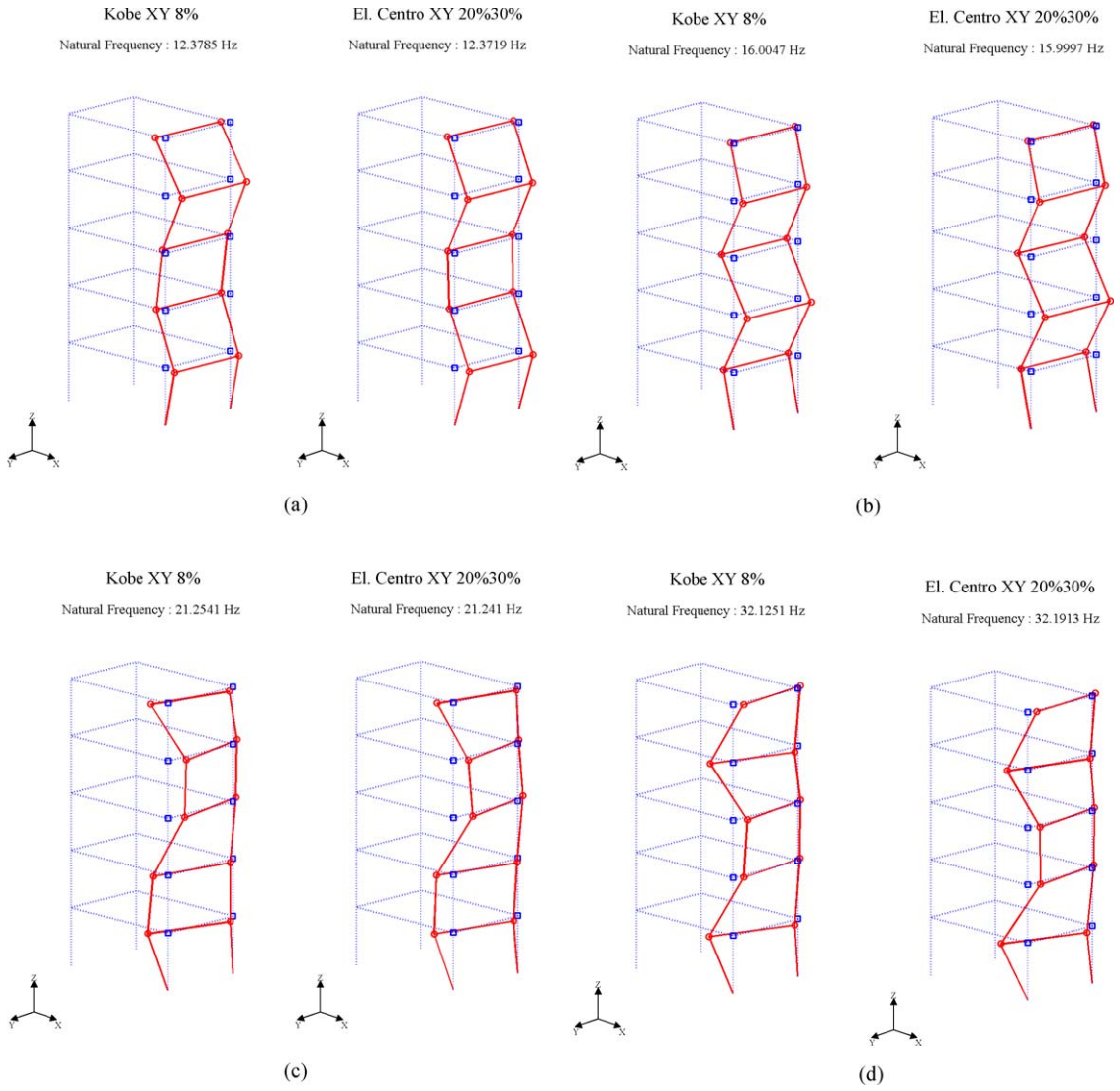

Fig. 9. Normal mode shapes in Kobe XY 8% and El. Centro XY 20%30% cases. (a) Mode 8 ($X4$); (b) Mode10 ($X5$); (c) Mode 12 ($T3$); (d) Mode 14 ($T4$).

model are backward difference models, and the difference between the two methods is in their inclusion of input data or not. The VBAR model can be regarded as a special case of the VBARX model without input data.

Acknowledgements

The authors thank the National Science Council (Taiwan) for financially supporting this research under Contract No. NSC 90-2611-E-002-027.

References

[1] R. Provasi, G.A. Zanetta, A. Vania, The extended Kalman filter in the frequency domain for the identification of mechanical structures excited by sinusoidal multiple inputs, *Mechanical System and Signal Processing* 14 (2000) 327–341.

[2] M.B. Tischler, System identification methods for aircraft flight control development and validation, *NASA Technical Memorandum 110369*, USAATCOM Technical Report 95-A-007, 1995.

[3] S.R. Ibrahim, E.C. Mikulcik, A time domain vibration test, *Shock and Vibration Bulletin* 43 (1973) 21–37.

[4] S.R. Ibrahim, Modal confidence factor in vibrating testing, *Journal of Spacecraft and Rockets* 15 (1978) 313–316.

[5] F. Deblauwe, D.L. Brown, R.J. Allemang, The polyreference time domain technique, *Proceedings of the Fifth International Modal Analysis Conference Society for Experimental Mechanics,* London, UK, 1987, pp. 832–842.

[6] J.M. Leuridan, D.L. Brown, R.J. Allemang, Time domain parameter identification methods for linear modal analysis, *Journal of Vibration, Acoustics, Stress, and Reliability in Design* 108 (1986) 1–8.

[7] F. Lemeregt, R. Snoeys, Application and evaluation of multiple-input modal parameter estimation, *International Journal of Analytical and Experimental Modal Analysis* 2 (1987) 19–31.

[8] J.N. Juang, R.S. Pappa, An eigensystem realization algorithm for modal parameter identification and model reduction, *Journal of Guidance, Control, and Dynamics* 8 (1985) 620–627.

[9] J.N. Juang, R.S. Pappa, Effect of noise on modal parameters identified by the eigensystem realization algorithm, *Journal of Guidance, Control, and Dynamics* 9 (1985) 294–303.

[10] P. Van Overschee, B. De Moore, N4SID: subspace algorithm for the identification of combined deterministic stochastic system, *Automatica (Special Issue on Statistical Signal Processing and Control)* 30 (1994) 75–93.

[11] M. Verhaegen, P. Dewilde, Subspace model identification. Part 1. The output-error state-space model identification class of algorithms, *International Journal of Control* 56 (1992) 1187–1210.

[12] P. Van Overschee, B. De Moor, A unifying theorem for three subspace system identification algorithms, *Automatica* 31 (1995) 1853–1864.

[13] D.A. Pierre, J.R. Smith, D.J. Thudnowski, J.W. Pierre, Based methods for simultaneous identification of transfer functions and initial conditions, *Computers and Electronic Engineering Prony* 21 (1995) 89–100.

[14] N.P. Mehta, S.M. Pandit, Modal analysis of multiple eigenvalue system by dynamic data systems, *Journal of Vibration and Acoustics* 113 (1991) 416–417.

[15] C.S. Huang, Structural identification from ambient vibration measurement using the multivariate AR model, *Journal of Sound and Vibration* 241 (2001) 337–359.

[16] R. Kumaresan, D.W. Tufts, Estimating the parameters of exponentially damped sinusoids and pole-zero modeling in noise, *IEEE Transaction of Acoustics, Speech, and Signal Processing* 30 (1982) 833–840.

[17] J.J. Hollkamp, S.M. Batill, Automated parameter identification and order reduction for discrete time series models, *American Institute of Aeronautics and Astronautics Journal* 29 (1991) 96–103.

[18] J.E. Cooper, The use of backwards model for structural parameters identification, *Mechanical System and Signal Processing* 6 (1992) 217–228.

[19] C.F. Hung, W.J. Ko, Identification of modal parameters from measured output data using vector backward autoregressive model, *Journal of Sound and Vibration* 256 (2002) 249–270.

[20] J.N. Juang, Applied System Identification, Prentice-Hall PTR, Englewood Cliffs, NJ, 1994.

[21] C.F. Hung, W.J. Ko, C.H. Tai, Identification of dynamic systems from data composed by combination of their response components, *Engineering Structures* 24 (2002) 1441–1450.

[22] W.J. Ko, C.F. Hung, Extraction of structural system matrices from an identified state-space system using the combined measurements of DVA, *Journal of Sound and Vibration* 249 (2002) 955–970.

[23] R.L. Allemang,D.L. Brown, A correlation coefficient for modal vector analysis, *Proceeding of the First International Modal Analysis Conference*, Bethel, CT, USA, 1983, pp. 110–116.

[24] D.J. Ewins, *Modal Testing: Theory and Practice*, Research Studies Press Ltd., London, 1984.

[25] S.C. Yeh, C.B. Zheng, C.H. Loh, Analysis report of shacking table test of the five-story 1/2-scale steel structure, *NCREE Research Report, NCREE-99-002*, 1999 (in Chinese).

[26] C.H. Loh, C.Y. Lin, C.C. Huang, Time domain identification of frames under earthquake loadings, *Journal of Engineering Mechanics* 126 (2000) 693–703.